J Therm Spray Tech (2017) 26:1548–1564
DOI 10.1007/s11666-017-0627-5

PEER REVIEWED

Optimization of Cold Spray Deposition of High-Density Polyethylene Powders

Trenton B. Bush[1] · Zahra Khalkhali[1] · Victor Champagne[2] · David P. Schmidt[1] · Jonathan P. Rothstein[1]

Submitted: 9 March 2017 / in revised form: 21 August 2017 / Published online: 1 September 2017

Abstract When a solid, ductile particle impacts a substrate at sufficient velocity, the resulting heat, pressure and plastic deformation can produce bonding between the particle and the substrate. The use of a cool supersonic gas flow to accelerate these solid particles is known as cold spray deposition. The cold spray process has been commercialized for some metallic materials, but further research is required to unlock the exciting potential material properties possible with polymeric particles. In this work, a combined computational and experimental study was employed to study the cold spray deposition of high-density polyethylene powders over a wide range of particle temperatures and impact velocities. Cold spray deposition of polyethylene powders was demonstrated across a range broad range of substrate materials including several different polymer substrates with different moduli, glass and aluminum. A material-dependent window of successful deposition was determined for each substrate as a function of particle temperature and impact velocity. Additionally, a study of deposition efficiency revealed the optimal process parameters for high-density polyethylene powder deposition which yielded a deposition efficiency close to 10% and provided insights into the physical mechanics responsible for bonding while highlighting paths toward future process improvements.

✉ Jonathan P. Rothstein
rothstein@ecs.umass.edu

[1] Department of Mechanical and Industrial Engineering, University of Massachusetts, Amherst, MA 01003, USA

[2] U.S. Army Research Laboratory, Weapons and Materials Research Directorate, Aberdeen Proving Ground, Aberdeen, MD 21005, USA

Keywords cold spray · fluid dynamics · polyethylene · polymer · polymer nanocomposites

Introduction

Developed first in the mid-1980s by Papyrin et al. (Ref 1), cold spray is a well-established additive manufacturing technique for coating and depositing a wide range of metallic materials. This technique utilizes a high-pressure gas stream to carry metallic powder particles through a converging-diverging Laval nozzle where they are accelerated to supersonic velocities before impacting on a solid substrate (Ref 2-5). The high-speed impact of these particles on the substrate can yield a variety of results depending on the particle velocity, impact angle, the size and shape of the particle, and the particle and substrate materials involved. This includes peening or permanent indentation of the substrate, erosion from the substrate, substrate abrasion, and, in the case of cold spray, the embedding of particle into the substrate with strong particle-substrate adhesion (Ref 6-8). What makes cold spray different from other thermal spray techniques is that during flight the particles remain in the solid state. Traditional thermal spray technologies where feed stock is melted before deposition are limited by a number of problems inherent to high-temperature processing. These include oxidation, phase change, compositional change, and residual stresses. Many of those problems are alleviated, if not entirely avoided, by the low-temperature, solid-state processing possible with cold spray (Ref 9, 10). In fact, cold sprayed metallic materials can have mechanical properties that equal or even surpass wrought materials (Ref 11). As a result, the cold spray process has become popular in the aerospace and other industries as a

mechanism for repair and reconditioning of metal parts (Ref 8, 11).

These technological advantages have motivated a flurry of research, both in industry and in academia, typically seeking to optimize or otherwise improve measures of coating quality or economic efficiency. A handful of recent studies have focused on expanding the range of deposit materials to include both polymeric materials and polymer nanocomposites (Ref 2, 12-15). Polymeric materials offer a tremendous range and variety of material properties. And, like metals, polymeric materials are subject to similar degradation issues associated with high-temperature processing. Cold spray processing appears to be an excellent candidate as a new green additive manufacturing technique for polymer materials as the polymeric powders can be processed in the solid state and without the use of toxic solvents.

The impact of polymer particles on a substrate differs significantly from that of metal particles due to the difference in mechanical properties, elastic modulus, thermal conductivity, degree of crystallinity, and the availability of metallic bonds to aid in adhesion (Ref 2). As a result, much is still unknown, including some very fundamental questions which we will investigate in this paper like what is a suitable range for the gas stream velocity for efficient particle deposition and how does this deposition window relate to the material properties of the particle and the substrate. A rule of thumb exists for the cold spray deposition of metallic particles, but it is unclear whether the same empirical formula for the critical impact velocity can be directly applied to polymer particles. Below this critical impact velocity, there is insufficient deformation and/or heating of the particle to ensure adhesion. Conversely, extreme impact velocities can induce stresses on the target that are large enough to overcome adhesion and strip the particles right off the substrate or even ablate the substrate (Ref 8). In this paper, we will use a combined computational and experimental study to map out a deposition window for the cold spray deposition of high-density polyethylene (HDPE) particles to investigate the role of particle temperature, impact velocity, and size on deposition efficiency and quality on a wide range of both polymeric and non-polymeric substrates.

Although the literature is sparse in this area, several studies have demonstrated successful cold spray deposition of polymer powders (Ref 2, 12-15). Xu and Hutchings (Ref 2) successfully deposited large (D = 150-250 μm) HDPE particles on an HDPE sheet. They reported critical impact velocity of just over 100 m/s which is an order of magnitude lower than for most metal sprays. At those impact velocities, a deposition efficiency less than 0.5% was reported (Ref 2). Note that this number is significantly lower than what has been reported for metals for which a deposition efficiency of nearly 100% is achievable (Ref 8). Xu and Hutchings noted that gross melting of the entire particle did not occur, but they could not rule out localized melting near the point of impact (Ref 2). Numerical simulations of HDPE polymer particle impacting an HDPE substrate performed by Shah et al. (Ref 15) reinforced these experimental observations and showed that at these impact velocities, a large temperature jump in the polymer was observed at the interface between the particle at the substrate resulting from the large shear stresses and plastic deformation of the polymer. In some cases, the temperatures attained were large enough to induce a local melting of the semicrystalline polymer and the mobilization of amorphous polymer chains in both the substrate and the particle. These thermal effects appear to be critical to aid interdiffusion and bonding between the plastically deformed particle and the substrate as Shah et al. (Ref 15) showed that the interfacial tension effects alone were not large enough to explain particle adhesion.

Alhulaifi et al. (Ref 14) designed a diffuser nozzle to deposit smaller HDPE particles (D = 53-75 μm) on an aluminum substrate and reported a critical velocity of 190 m/s. Deposition on aluminum proved difficult and required substantial heating of the aluminum substrate to be successful. The simulations of Shah et al. (Ref 15) showed that the initiation of an initial deposition on the aluminum substrate is likely the limiting step as the presence of a thin melted layer of polymer on a hard substrate resulted in a significant increase in plastic deformation and energy dissipation in the polymer upon particle impact.

Alhulaifi et al. (Ref 14) did not report deposition efficiency for their experiments. Ravi et al. (Ref 13) deposited ultra-high molecular weight polyethylene (UHMWPE) onto both aluminum and polypropylene substrates. In their experiments, a thick coating was only possible by deploying a 4 wt.% alumina nanoparticle additive to aid in inter-particle bonding. Additionally, they analyzed the thermal history of rebound, adhered, and unsprayed UHMWPE powder by differential scanning calorimetry (DSC), finding that only the adhered particles displayed evidence of melt crystallization. They did not report either the critical impact velocity or the deposition efficiency (Ref 13). The simulations of Shah et al. (Ref 15) showed that the addition of metallic nanoparticles to the polymer particle improved the likelihood of deposition by increasing the particle's density and its impact kinetic energy for a fixed impact velocity.

Understanding the mechanics of particle deposition is critical to the design and optimization of the processing conditions. For metal deposition, various ideas for bonding mechanisms have been proposed and examined over the past 15 years (Ref 16). Assadi et al. (Ref 17) were the first to discover a necessary but not sufficient criterion for

deposition: During particle impact, plastic strain energy is released locally as heat, which softens the material and encourages further deformation and heat release. This positive feedback condition, termed the adiabatic shear instability, occurs at high strain rates where the rate of thermal softening exceeds the rates of strain and strain-rate hardening. This condition is also likely necessary for polymer particle deposition. Assadi et al. (Ref 17) proposed that the extensive deformation and heating at the interface disrupted oxide layers and allowed the formation of metallic bonds between particles and substrate which aid adhesion. Unfortunately, for most polymers, the formation of metallic bonds and thus other bonding mechanisms must be at work to achieve particle deposition.

Due to the sheer diversity of material combinations involved, no single adhesion mechanism is capable of explaining all metal cold spray experimental results. Most studies have provided support for mechanisms based on either topochemical reactions or mechanical interlocking (Ref 16, 18-21). For example, Li et al. (Ref 18, 19) concluded that most metals likely experience local melting at the particle interfaces. Recent numerical simulations of Shah et al. (Ref 15) for polymer particle impacts also support the idea of localized particle melting. However, the process under which melting occurs and the properties that result differ across materials. Low melting point, high gas temperature, atmospheric reaction/oxidation, and/or poor thermal conductivity could all play a role in the localized melting of the particles. Mechanical mixing between the particle and substrate interface is thought to partially explain adhesion for ductile particles (Ref 22) due to an interfacial flow instability between two materials of different viscosities (Ref 23). However, Klinkov et al. (Ref 20) noted that a mechanical mixing mechanism could not account for successful coatings on brittle glass and ceramic substrates. For those systems, a mechanism based on simultaneous impacts was statistically unlikely and did not match observed deposition efficiencies. They concluded that the mechanism of topochemical reactions held the greatest explanatory value due to its ability to account for size and velocity dependence of deposition efficiency and for the existence of an 'incubation time' during which the substrate surface is activated by impinging particles (Ref 20). These observations can also be extended toward polymeric particles where the materials brittleness and ductility can depend on both polymer microstructure and crystallinity as well as its temperature with more amorphous polymers behaving more like viscoelastic liquids or metallic glasses (Ref 24, 25) upon impact and more crystalline polymers, like HDPE, behaving more like crystalline metals.

In a novel proposition, Hussain et al. (Ref 21) suggested a combined mechanism based on a modified composite strength model, with one fraction of interfacial area joined by metallurgical bonding and another fraction by mechanical interlocking. By using surface preparations to vary the ratio of metallic bonding to mechanical interlocking, the authors reported that mechanical interlocking was able to account for a large proportion of the total bond strength. For their experiments (copper on aluminum alloy), metallic bonding dominated only on a polished and annealed surface where the fraction of metallic bonding approached 100% (Ref 21). For an extensive review of many proposed bonding mechanisms, see Hussain (Ref 16). These experiments give optimism for polymer cold spray as mechanical interlocking, not the formation of metallic bonds, is expected to dominate adhesion for nearly all polymeric materials.

In the present work, we seek to further the flexibility and capability of the cold spray technology for depositing polymers. We will present a series of computation fluid dynamics simulations which were used to optimize the design of a converging-diverging nozzle to maximize the total energy, kinetic plus thermal energy, in the polymer particles upon impact while insuring a temperature above the melt temperature. In order to study cold spray deposition of polymeric material, a complete spray system was designed and built starting from the nozzle design and working upstream. We will present our findings for the deposition window for HDPE particles on a series of polymeric and non-polymeric substrates. We will present our findings of the deposition efficiency (DE) as a function of parameters such as hopper temperature, particle impact velocity, nozzle standoff distance, substrate material, and bed temperature. Finally, we will discuss how these parameters can be further optimized to maximize deposition efficiency in future studies where particle design can be closely integrated with the process parameters.

Experimental Setup

Nozzle Design

The nozzle profiles found in the literature and implemented in commercially available cold spray systems were optimized for metal powders. Additionally, they were designed for commercial use and, as a result, required either powerful compressors or large volumes of stored gas to sustain their high volume flow rates. By reducing throat diameter to $D_T = 1.6$ mm, the volume flow rate of gas (air or nitrogen) was brought down to research scale and could be operated on either a consumer-grade air compressor or a high-pressure nitrogen bottle.

Several different nozzles were designed and tested for this study. The initial nozzle design was informed by the

experimental results of Xu and Hutchings (Ref 2) and based on the critical velocity equation of Schmidt et al. (Ref 2, 3) which states that the critical impact velocity for adhesion scales like the following

$$v_{cr} = \sqrt{F_2\, c_p\left(T_m - T_p\right) + F_1\, \frac{4\sigma}{\rho}\left(\frac{T_m - T_p}{T_m - T_{ref}}\right)}. \qquad \text{(Eq 1)}$$

Here, F_1 and F_2 are empirical fitting constants, T_m is the melt temperature of the particle, T_p is the temperature of the particle at impact, T_{ref} is the temperature at which particle material properties were measured, σ is the tensile strength of the particle, ρ is the density of the particle, and c_p is the specific heat of the particle. The critical velocity model of Eq 1 is a weighted combination of two different models used to understand the dynamics of particle impact and adhesion (Ref 3). In the first part of Eq 1, the critical impact velocity is associated with a certain fraction, F_2, of the impact kinetic energy being converted entirely into thermal energy

$$\frac{1}{2}\rho_p v_{cr}^2 = F_2 \rho_p c_p \left(T_m - T_p\right). \qquad \text{(Eq 2)}$$

The second part of Eq 1 is dynamical model correlates the ground pressure resulting from the ballistic impact of the particle to the tensile strength of the particle with a correlation coefficient, F_1, such that

$$\frac{1}{8}\rho v_{cr}^2 = F_1\, \sigma\left(\frac{T_m - T_p}{T_m - T_{ref}}\right). \qquad \text{(Eq 3)}$$

Here, the tensile strength of the particle is modified using the Johnson–Cook equation to account for thermal softening. For metal cold spray, a wide range of materials have been studied and it has been shown that the critical impact velocity data from across all these materials can be collapsed when $F_1 = 1.2$ and $F_2 = 0.3$ (Ref 3), resulting in an empirical formula for the critical impact velocity for adhesion that becomes

$$v_{cr} = k\sqrt{c_p\left(T_m - T_p\right) + \frac{16\sigma}{\rho_p}\left(\frac{T_m - T_p}{T_m - T_{ref}}\right)}. \qquad \text{(Eq 4)}$$

For metal-on-metal deposition, the fitting parameter in Eq 4 has been found to be $k = 0.55$ (Ref 3). Using the material properties of HDPE and the fitting coefficient from metal cold spray, a critical impact velocity of approximately 400 m/s is expected at room temperature. This is equivalent to a Mach number in air of $Ma = 1.16$ which is significantly lower than what is needed for metals due to the lower specific heat and tensile strength of HDPE as compared to even soft metals such as copper. As a result, the converging-diverging nozzle design for polymer cold spray can be designed with a much smaller area ratio than a typical metal cold spray nozzle.

A one-dimensional (1D) inviscid model of gas and particle dynamics created by Champagne et al. (Ref 26) was used for rapid prototyping and as the basis for a numerical optimization routine with which three of the nozzles were designed. The model uses 1D compressible gas dynamics theory to calculate the velocity, temperature and pressure variations through the nozzle (Ref 27). In a converging-diverging nozzle, the gas is accelerated to the speed of sound at the throat and then supersonic, $Ma > 1$, in the diverging section of the nozzle by converting the enthalpy of the gas into kinetic energy. As a result, as the velocity increases, the pressure and temperature of the gas decrease in a known way that is easily calculated from theory (Ref 27). The particle velocity is determined by first assuming the particles do not disturb the flow field and then calculating the drag force using a simple drag law. The temperature of the particle is similarly calculated by finding the convective heat transfer coefficient from the particle motion and then calculating the heat transfer rate and particle temperature as a function of position along the nozzle assuming a lumped capacitance model. A detailed description of the mechanics behind the simplified model, including a comparison to computational fluid dynamics (CFD) simulations and experimental results, is available from the original authors (Ref 26). This assumption of constant temperature within the particle is valid for metal particles because the Biot number is quite small owing to the large thermal conductivity of the metal particle. However, this assumption breaks down for HDPE and other polymers as their thermal conductivity is much smaller. For impact velocities targeted here, the resulting Biot number was calculated to be slightly larger than lumped capacitance cutoff of $Bi \sim 0.1$ (Ref 28). As a result, the particle temperature will deviate from uniform and a modest temperature distribution of a few degrees (between 4-8 °C depending on processing conditions) will exist across the particle with the outer shell of the particle becoming cooler than the core during its flight through the nozzle. Fortunately, for the purposes of nozzle design, the detailed temperature distribution within the particle is not critical to calculating the relative loss in thermal energy in the particles as the average temperatures of the particles remain nearly identical. Therefore, for ease of calculations, we chose to use the lumped capacitance model in both 1D theoretical predictions of nozzle performance and the 2D CFD simulations which were run to validate the 1D model and finalize the nozzle designs. For the purposes of particle impact simulations, a more precise 3D temperature profile across the particle upon impact might be critical to accurately model the temperature distribution within the particle during impact.

The cold spray nozzle designs were all modeled, meshed, and solved with a commercially available CFD

code, ANSYS Fluent®. The nozzle geometries were all modeled as axisymmetric. The exit domain of the nozzles was designed to be large enough (20 times the outlet radius) to sufficiently isolate the outlet boundary from the jet, allowing us to impose an exit boundary condition set to room temperature and pressure. The inlet boundary was placed upstream of the converging portion of the nozzle ($\sim$2.5 times the inlet radius) to allow flow to develop before reaching the nozzle and set to the experimental inlet gas conditions. All cases were meshed with mapped quadrilaterals from the nozzle inlet through the nozzle and free jet to the substrate. Unstructured meshing, again with quadrilaterals, was used to fill out the extended domain around the free jet to the outlet boundary. Mesh size was refined in areas where high gradients were anticipated, such as the nozzle throat, diverging section, free jet region, and substrate surface. A grid independence test was performed on a representative case and resulted in a mesh of approximately 70,000 cells. A RANS k-ε RNG model was used to model the high Reynolds number flow. The working fluid was air and was modeled as a compressible ideal gas, with viscosity dependent on temperature via the three coefficient formulation of Sutherland's Law. Material properties were sourced from the Fluent materials database and the defaults chosen. Nozzle and substrate walls were treated as no-slip and adiabatic boundaries. Both the flow and turbulence equations were solved with a second-order upwind scheme. For cases with supersonic flow, the flux vectors were computed via the Advection Upstream Splitting Method (AUSM). This vector splitting method allows for exact resolution of shock discontinuities, preserves positivity of scalar quantities, and is free of oscillation for both stationary and moving shocks. This is ideal for supersonic flow. For subsonic flows, the Roe Flux-Difference Splitting Scheme was used because it provided better stability and faster convergence. Once a solution to the gas flow field had been obtained, particle motion was introduced via a Lagrangian discrete phase model. Interphase interaction was limited to acceleration of and heat transfer to the particle only. A single particle with a diameter of 48 μm was released along the nozzle axis, propelled through the flow field via Fluent's high Mach number drag law. This drag law applies corrections to the spherical drag law when particle Mach number is greater than 0.4 or particle Reynolds number exceeds 20.

The results of the CFD simulations agreed quite well with the 1D theory within the nozzles, but downstream of the nozzle exit, the 2D CFD simulations were able to provide additional insight into particle trajectories as they interacted with oblique shocks and expansion waves due to under- or over-expansion of gas as it exited the nozzle and bow shock waves set up at the substrate. This can be seen in Fig. 1 for a converging nozzle designed to accelerate particles to supersonic velocity before impacting a substrate. In Fig. 1, a series of Mach diamonds are visible as the pressure conditions resulted in a slightly over expanded gas. Upon impacting the substrate, a standing bow shock wave can be observed. Although the Mach diamonds were found to have a large effect on the gas flow, deflecting the gas up and down by as much as 10 degrees as the gas passed through each successive diamond, the inertia of the particles was enough to maintain a fairly straight path toward the substrate. Note that both the particle velocity and temperature lagged those of the gas. In Fig. 1, the particles were found to reach a velocity of just under 300 m/s, while the gas reached more than 600 m/s.

The design of the nozzles for polymer cold spray took the particle temperature/impact velocity tradeoff into account to maximize the likelihood of adhesion. The hypothesis was that high-velocity carrier gas produced relatively cold, hard particles that were difficult to deform, and that the high stagnation pressures and shock phenomena that accompany high-velocity carrier gas could strip away some deposits, negatively impacting deposition efficiency. Thus in meeting the deposition criterion, this hypothesis would suggest that the ideal nozzle should maximize particle temperature at impact to reduce the critical impact velocity needed. A hotter, softer particle would require a less energetic impact to achieve the level of plastic deformation necessary for deposition. This reduction in the required particle velocity would allow reduced gas velocity and pressure. Numerical optimization was performed via a Generalized Reduced Gradient (GRG) method. For the 'Max Temp' nozzle, the parameters varied were area ratio and length of the diverging section with the design constraints limited by available tooling and maximum pressures and volume flow rate of the carrier gas.

A second nozzle design ('Max Velocity Match') nozzle was designed to maximize particle velocity with two key constraints: (1) maximum compressor pressure of 5 bars and (2) static pressure at the nozzle exit equal to atmospheric pressure (to minimize shock phenomena at nozzle exit). The design principle was to use a standard converging-diverging nozzle to expand the gas until the atmospheric pressure constraint was reached, and then channel the supersonic gas stream through a constant-area extension to maximize particle residence time and thus velocity. This geometry produces Fanno flow conditions, resulting in a normal shock in the constant-area extension that decelerated (and heated) the gas back to sonic conditions. In this design, the particles are rapidly accelerated by supersonic flow and then are conveyed by warmer sonic gas, and the substrate is not subjected to shock phenomena as in standard converging-diverging nozzles. This result is similar to that of the diffuser nozzle created by Alhulaifi

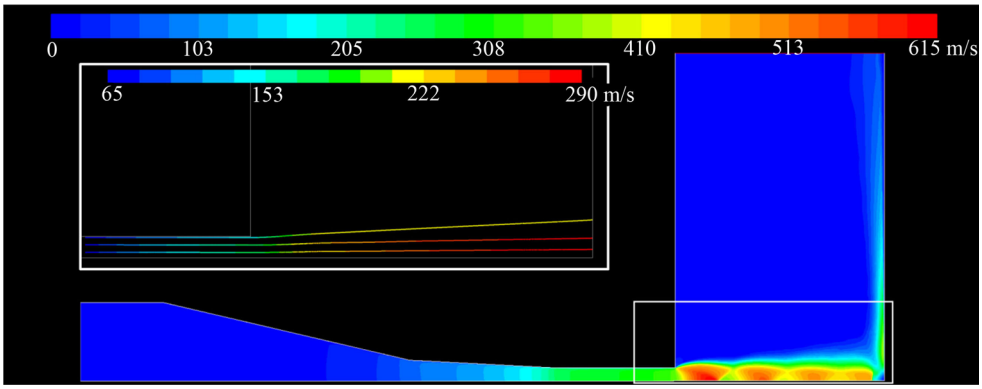

Fig. 1 CFD simulations showing velocity magnitude contours of the flow through a converging nozzle with a 6:1 contraction ratio and a final exit diameter of 0.16 cm operating with a 5 bar inlet pressure, an inlet temperature of 295 K and a standoff distance of 12.7 mm from the substrate. The inset shows the particle paths with color scaled by particle velocity for as series of 23-μm-diameter particles released just upstream of the inlet with an initial velocity equal to flow at the location they were released

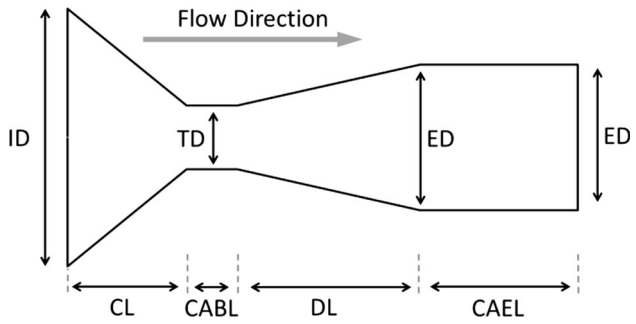

Fig. 2 Schematic diagram of the axisymmetric nozzle geometry. See Table 1 for dimensions. Abbreviations correspond to the following: inlet diameter (ID), throat diameter (TD), exit diameter (ED), converging length (CL), constant-area buffer length (CABL), diverging length (DL), and constant-area extension length (CAEL)

et al. (Ref 14), but without the complications of a second throat.

The nozzles were fabricated by initially drilling a 1.6-mm pilot hole through a length of 6061 aluminum rod. Tapered end mills were then used to cut the converging and diverging portions resulting in the nozzles shown schematically in Fig. 2. The optimized diverging length of the high-speed Max Energy nozzle necessitated a diverging angle of 1.4° which is an angle not available for tapered endmills. The nearest tapered endmill angle was 3°, which necessitated the inclusion of a new constraint into the optimization routine and a re-optimization of the length.

After preliminary results showed that deposition could be achieved at much lower particle velocities than predicted by Eq 1, a final nozzle ('Min Velocity') was created to test the lower boundary of deposition. This nozzle, like the 'Max Temperature' nozzle, operated on the principle of low-velocity, high-temperature particle impacts. It is merely a shortened version that produces even slower, hotter particles. The 'Min Velocity' nozzle was used to determine the critical impact velocity for all results that follow while the 'Max Temperature' and 'Max Velocity Match' where used to explore the upper limits of impact velocities at supersonic particle velocities.

Cold Spray Setup

A cold spray system was designed and built to utilize the nozzles designed in the previous section. A schematic diagram of the cold spray system, and specifically the hopper design, is presented alongside an image of the actual setup in Fig. 3. As described in the previous section, due to the lower anticipated critical impact velocity, it was possible to run this polymer cold spray system either using a compressed nitrogen cylinder or a 1.85 kW, consumer-grade single-stage air compressor capable of producing a pressure of 6.2 bars at 8.5 m^3/h. The compressed air traveled through filters and a pressure regulator before entering a heated pressure vessel which housed the powder feeder. The hot gas/powder mixture then exited the vessel and passed through the nozzle. This spray system emphasizes powder preheating with a linear system design. The powder and process gas are heated together and mixed well upstream of the nozzle. Unlike many commercial systems, there is no parallel routing of cold powder-conveyor gas that must be mixed at the nozzle entrance.

The aluminum pressure vessel was heated with three 500 W band heaters (Omega MB-1). The temperature of the pressure vessel was monitored with an internal bore thermocouple (Omega BT) inserted through a radial pressure fitting near the bottom of the barrel and was controlled with a PID temperature controller (Omega CN2110). The inner diameter of the pressure vessel was 38 mm, and it had a total length 27 cm. Nozzle inlet conditions were monitored via a thermocouple and a pressure transducer (Omega PX309-300GV) inserted just upstream of the nozzle as seen in Fig. 3(b). At the mass flow rates

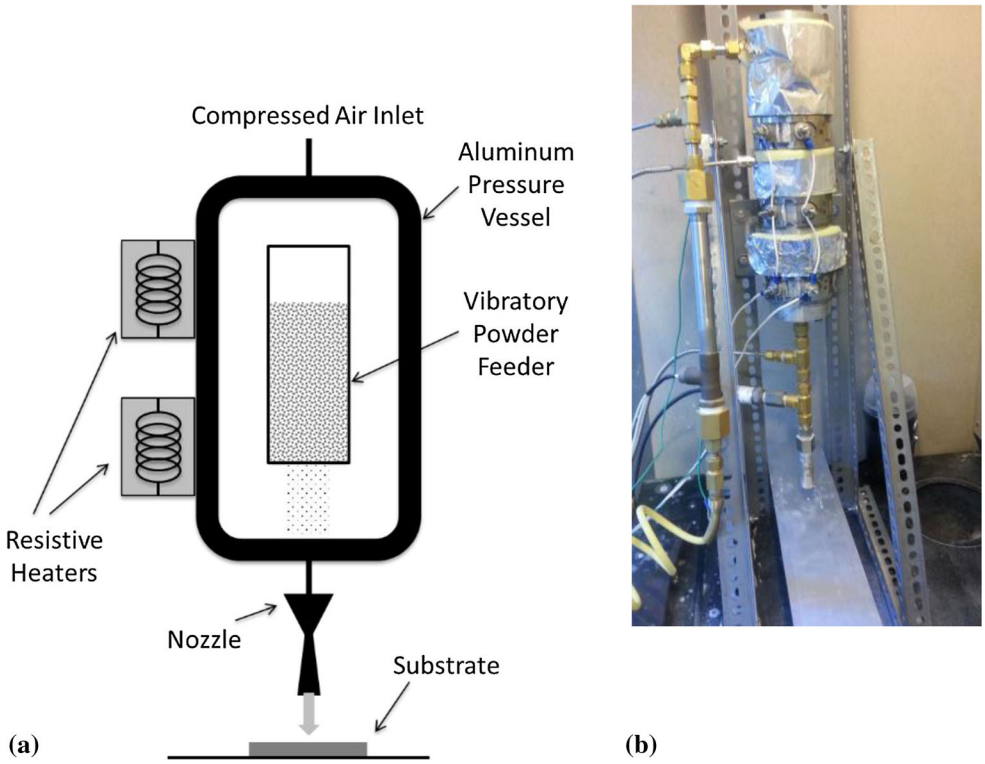

Fig. 3 (a) Schematic of research-scale cold spray system and (b) photography of the actual setup

Table 1 Dimension of the three nozzles used in this study

Geometry	Max temperature nozzle	Min velocity nozzle	Max velocity match nozzle
Inlet diameter, cm	0.95	0.95	0.95
Throat diameter, cm	0.16	0.16	0.16
Exit diameter, cm	0.16	0.16	0.19
Converging length, cm	2.39	2.31	2.99
Constant-area buffer length, cm	2.60	0.72	0.07
Diverging length, cm	N/A	N/A	0.30
Constant-area extension length, cm	N/A	N/A	4.19
Area ratio	1.00	1.00	1.45
Maximum inlet pressure, kPa	496	496	496
Maximum mass flow rate of air, g/s	0.67	0.67	0.67
Maximum particle velocity, m/s	237	250	459

'Max Temperature' to maximize particle temperature, 'Min Velocity' to explore minimum deposition velocity, and 'Max Velocity Match' to generate the maximum velocity such that nozzle exit pressure matched atmospheric pressure

employed by this cold spray system in this study, the residence time of the air within the heated pressure vessel was sufficient to heat the air up to the controlled temperature of the pressure vessel which could easily exceed 150 °C. The measured inlet temperature and pressure conditions were used as inputs to the CFD code to simulate the nozzle flow field so that the particle impact conditions could be calculated and the data presented as a function of particle and not gas temperature and velocity.

Powder feed was accomplished by routing the carrier air around a vibratory powder dispenser contained in the pressure vessel. A pneumatic vibrator (Cleveland Vibrators VM-25) was mounted on a connecting rod above the pressure vessel. The connecting rod ran through a slip-fit bushing and into the vessel, where it transmitted vibration to an attached aluminum tube that contained the powder to be deposited. The bottom of the tube was capped with coarse wire mesh, which allowed agitated powder to fall

into the surrounding carrier gas. Finally, a spring was mounted on the vibrating assembly in order to prevent pressurized air from pushing the connecting rod out of the pressure vessel. A schematic can be seen in Fig. 3. The hopper design is capable of delivering a wide range of particle feed rates depending on the mesh size chosen and the intensity of the vibratory agitation.

A 2D xy-stage was fabricated and controlled by an Arduino operated by an open source software package designed for 3D printing (Repetier-Host). A PCB heater was placed on top of this stage to enable controlled substrate heating up to 120 °C during deposition. The desired deposition patterns were inputted into the software as STL files. The stage speed could be varied from 1 to 20 mm/s to change the thickness and height of the deposited cold sprayed lines.

Materials

The powder deposited in this study was a commercially available high-density polyethylene (HDPE) powder (BYK Ceraflour 916). The powder size was quite polydisperse with a mean diameter of $d_{50} = 48$ μm with a standard deviation of 18 μm and a percent crystallinity between 70 and 80% according to the manufacturer. Differential scanning calorimetry (DSC) measurements showed a peak melt temperature of $T_m = 127.8$ °C. Note, however, that the particles were found to become tacky at temperature well below the melt temperature. As a result, the particles were found to jam in the hopper at temperatures above 70 °C, thus setting the maximum operating temperature of the pressure vessel for this powder. The density of the particles was $\rho = 0.99$ g/mL.

Cold spray deposition of the HDPE was studied on a series of both polymeric and inorganic substrate materials. These include high-density polyethylene (HDPE) (Vycom Hitec), polyvinylchloride (PVC) (Vycom Vintec 1), polyoxymethylene (POM) (Quadrant Acetron GP Acetal), melt-cast BYK Ceraflour 916, low-density polyethylene (LDPE) (McMaster-Carr), 6061 aluminum, and quartz glass. In the melt-cast case, BYK Ceraflour 916 powder was melted on an aluminum block over a hot plate, then pressed flat to a thickness of approximately 1 to 2 mm and allowed to cool. The relevant material properties of each of the substrate materials are presented in Table 1.

Results and Discussion

A series of experiments were performed in order to study how a number of key parameters affect the cold spray deposition of HDPE powder on to a number of different substrates. These parameters included particle temperature, size, and impact velocity; surface composition and temperature; as well as nozzle design and standoff distance. The effect of parameter variation on cold spray deposition were quantified by (1) determining whether deposition occurred or not, (2) by measuring the deposition efficiency and by characterizing the quality of the deposition through optical microscopy and scanning electron microscopy (SEM) images, and (3) quantification of the porosity of the deposition and measurements of the material of the deposited HDPE through tensile testing and nano-indentation (Table 2).

Window of Deposition Studies

Like-on-Like Deposition

The first sets of experiments performed were designed to set a baseline for future comparisons by studying the deposition of HDPE powders on a melt-cast surface of the same HDPE powder. Two different nozzles were utilized and compared against each other: the Max Temperature Nozzle and the Max Velocity Match Nozzle. In these experiments, the nozzle standoff distance was set to 20 mm and the substrate was held at room temperature. A number of different hopper temperatures were utilized between 20 and 80 °C and pressures between 1 and 2 bars resulting in particle velocities that ranged from 75 to 275 m/s. In Fig. 4, the resulting window of deposition for like-on-like deposition of the HDPE powder is shown for a nozzle

Table 2 Material and empirical fitting properties

Substrate material	Yield strength, MPa	Density, kg/m^3	Shore D hardness	Fitting constant, k
Melt-cast HDPE	20	990	N/A	0.187
HDPE	31.7	960	69	0.152
LDPE	14.6	920	50	0.147
POM	65.5	1410	85	0.172
PVC	88.2	1420	89	0.153
Copper on copper	50-85*	8960*	N/A	0.548

Copper on copper properties are provided for reference. Material properties marked with (*) are estimates for general material types. All others are from manufacturer data sheets

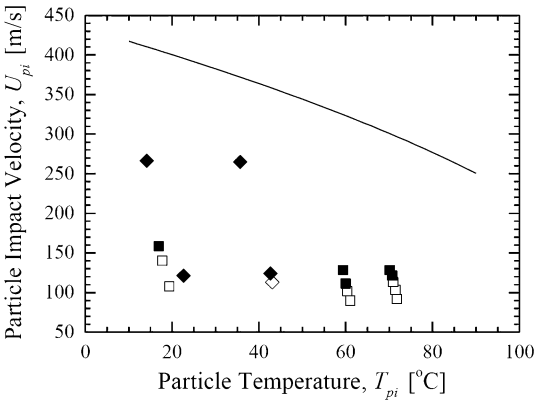

Fig. 4 Map of the cold spray deposition window for $D = 48$ μm HDPE particles. The data include results from two nozzles: (■) Max Temperature Nozzle and (◆) Max Velocity Match Nozzle. The filled symbols represent successful deposition and hollow symbols represent failed deposition. In these experiments, the nozzle standoff distance was set to 20 mm and the substrate was at room temperature. A solid line is superimposed over the data representing the predictions of the theoretical critical impact velocity from the model derived for the deposition of metal particles in Eq 3

standoff distance of 20 mm and an unheated, room temperature substrate. As is typical in the cold spray literature, the data are presented as particle temperature against particle impact velocity. Both the temperature and impact velocity were calculated using the inlet conditions to feed the CFD simulations so that the results would be independent of the design of the cold spray system. Here, only the lower boundary of the deposition window is visible. Experiments at velocities high enough to determine the upper boundary were not performed for this powder/substrate combination. Note also that once the particle impact velocity and temperature are calculated from the CFD simulations, there does not appear to be a clear advantage for using either of the nozzle designs tested here.

As expected, the critical particle impact velocity decreases with increasing hopper and particle temperature. Here, we observe a reduction from $U_{\text{crit}} = 140$ m/s at $T_{\text{pi}} = 20$ °C to $U_{\text{crit}} = 110$ m/s at $T_{\text{pi}} = 70$ °C. However, note that the critical impact velocity at room temperature predicted by Eq 4 exceeds the observed value by a factor of 3. As we will show in the next section, the data in figure can still be well fit by the model in Eq 4 if the fitting parameter, k, is modified from $k = 0.55$, which has been shown to work for metals, to $k = 0.19$ for this HDPE powder. This finding of significantly reduced critical impact velocity is consistent with previous studies of polyolefin deposition (Ref 2, 14). Clearly, the mechanics that govern adhesion in metal cold spray differ considerably from the polymer case. Taken in the context of the adiabatic shear instability mechanism, low thermal diffusivity is one possible explanation for the reduced critical velocity seen in polymers. Thermal diffusivity can be a thousand times lower in polymers than metals. As a result, temperature buildup at the interface may be more localized in a polymer than a metal particle (Ref 29, 30). This can be observed in the numerical simulations of Shah et al. who investigated the impact polymer particles on different substrates (Ref 15). Localization of the temperature rise could result in a reduction of the amount of total energy needed to be released through plastic deformation of the particle to obtain the interfacial temperature necessary for adhesion.

Surface topology was examined via optical microscopy and scanning electron microscopy (SEM) (FEI Magellan 400 XHR-SEM). Several deposition conditions were examined from a top view, 45 degree tilt, and in cross section. A small subset of these images is presented in Fig. 5. In all cases, the deposits were very similar. As can be seen from Fig. 5, a smooth continuous line was deposited in each case for inspection through SEM. Both in the optical images and the SEM images, no obvious grain boundaries between individual particles could be observed. For the size of the particles deposited, $D = 48$ μm, and the scale of the SEM images, each image should show impact craters of multiple particles. However, no evidence of individual particles is apparent from either the optical images or the SEM images in Fig. 5. Instead, the resulting HDPE deposition was found to be uniform and dense with little to no observable porosity or voids. The deposition was also found to be quite smooth with an average surface roughness of less than 10 μm, which is well below the diameter of the impacting HDPE particles. One possible explanation for the high quality of the deposition is that, as we will describe below, the deposition efficiencies were less than 10%. As a result, the particles that did not adhere may have been responsible for peening the deposition into a dense and smooth formation.

Deposition on Various Substrates

In order to better understand cold spray deposition of HDPE powders, deposition experiments were performed on both polymeric and non-polymeric substrates. For deposition of HDPE on non-HDPE polymeric substrates, adhesion can still be promoted by polymer mixing and entanglement. However, for successful deposition on non-polymeric substrates like aluminum and glass, particle adhesion will have to rely on energy dissipation due to plastic deformation of the particle and a large growth in the interfacial energy resulting from significant deformation and spreading of the impacting particle on the substrate. It is known that a large mismatch in the modulus of the particle and the substrate can lead to enhanced particle or substrate deformation and higher likelihood of adhesion (Ref 15, 31). Bae et al. (Ref 31) performed a combined

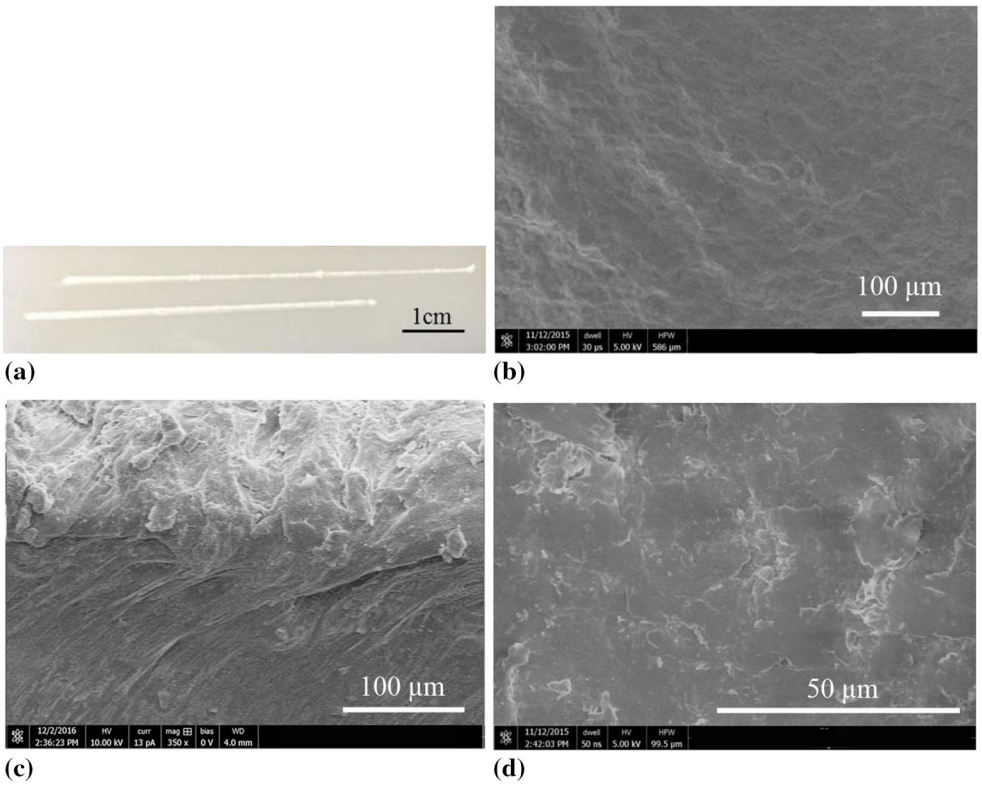

Fig. 5 Optical and SEM imaging of like-on-like cold spray deposits of 48 µm HDPE powders. In (a), an optical image of a 1D line of HDPE deposited at $T_{pi} = 19$ °C at $U_{pi} = 197$ m/s is shown. In (b), an SEM image of the top of the deposition in (a) is shown. In (c), the deposit in (a) was cut and imaged using SEM at a 45° angle to reveal the cross section of the deposit. In (d), an optical image of a 1D line of HDPE deposited at $T_{pi} = 17$ °C at $U_{pi} = 228$ m/s is shown

FEA and experimental study of metallic deposition and demonstrated that critical velocity decreases both when the substrate is harder and when it is softer than the impacting particle. They showed that when the particle was softer than the substrate, the particle experienced most of the plastic deformation, which created a greater contact area and higher interface temperature compared to the matched-hardness case. When the particle was harder than the substrate, the substrate underwent the more severe deformation, but again produced greater contact area and higher interface temperature compared to the matched-hardness case (Ref 31). Similar results were found by Shah et al. (Ref 15) who simulated the impact of polymer particles on both polymeric and metallic substrates with various elastic moduli.

Four different polymeric substrate materials were utilized, including the melt-cast HDPE described previously, along with sheets of commercially available HDPE, POM and PVC. The main difference between the melt-cast HDPE and the HDPE sheet was that, according to the manufacturer, the particles contained some amount of low molecular weight HDPE wax blended into a high molecular weight HDPE matrix. As a result, the modulus and yield strength of the HDPE particles and the resulting melt-cast substrate were lower than those of the HDPE sheets. See Table 1 for details. Cold spray deposition was performed with a nozzle standoff distance of 20 mm and the substrate at room temperature. A number of different hopper temperatures were utilized between 20 and 80 °C and pressures between 1 and 3 bars, resulting in particle velocities that ranged from 75 to 275 m/s. The resulting deposition maps are presented in Fig. 6. Successful cold spray deposition of HDPE was achieved on all four of these polymeric substrates. This is in stark contrast to our deposition attempts on inorganic substrates like aluminum and glass, for which successful deposition was not possible under these deposition conditions. As a result, the deposition map for aluminum and glass is not presented in Fig. 6. As will be shown in the following section, cold spray deposition of HDPE was possible on aluminum and glass, but required heating of the substrate up to the melting temperature of the HDPE powder to be successful.

In Fig. 6(a) and (c), cold spray deposition is presented on both the melt-cast HDPE and sheet HDPE substrates. In both cases, the chemistry of the substrate and the particle are the same. However, the modulus and hardness of the sheet HDPE are larger than those of the melt-cast HDPE due to its partial wax content. As seen in Fig. 6, the result

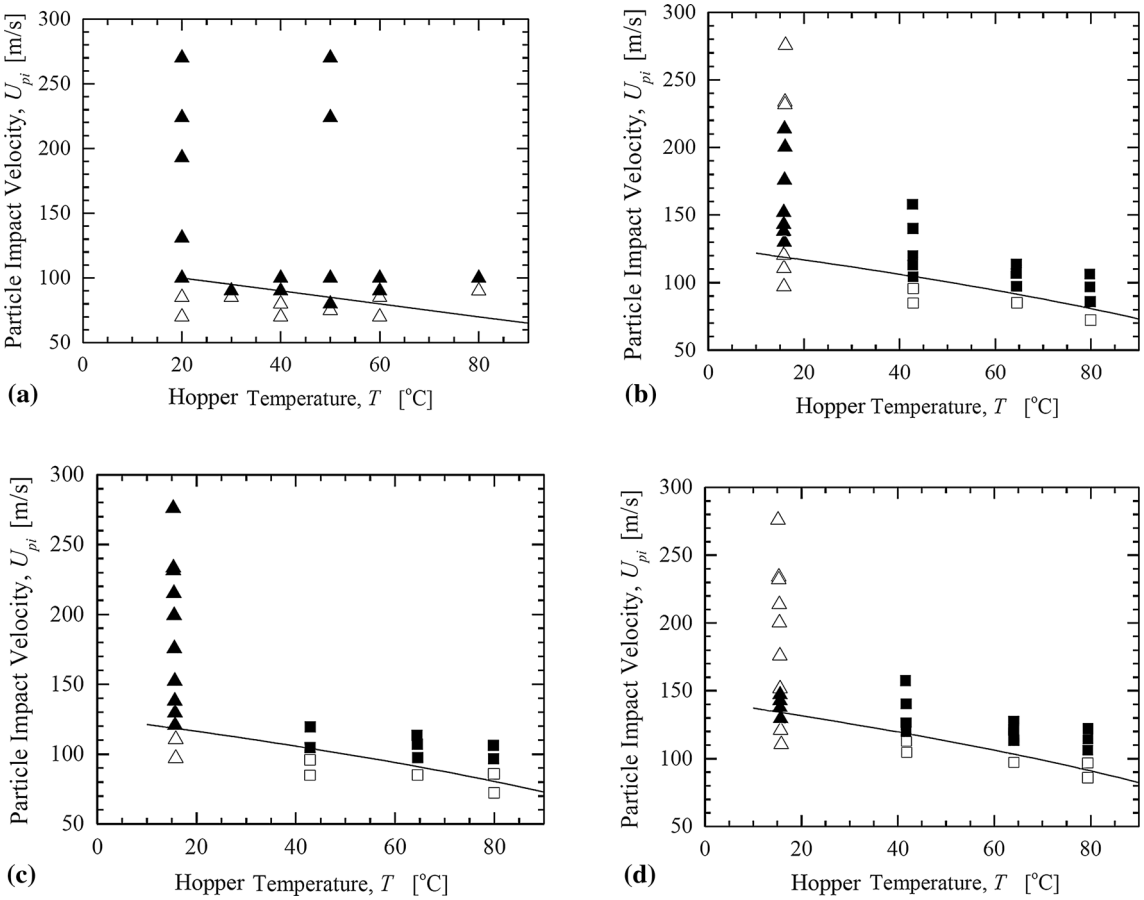

Fig. 6 Map of the cold spray deposition window for $D = 48$ μm HDPE particles on a variety of substrates including: (a) LDPE, (b) PVC, (c) HDPE, and (d) POM. The data include results from three different nozzles: (■) Min Velocity Nozzle, (◆) Max Temperature, and (▲) Max Velocity Match Nozzle. The filled symbols represent successful deposition, and hollow symbols represent failed deposition. In these experiments, the nozzle standoff distance was set to 20 mm and the substrate was at room temperature. A solid line is superimposed over the data representing the predictions of the theoretical critical impact velocity from Eq 3 where the constant k was varied to provide a best fit to the data

of the mismatch in modulus between the particle and the substrate was a reduction in the critical impact velocity across the entire temperature range of approximately 15%. As an example, at $T_{pi} = 20$ °C the critical impact velocity was reduced from $U_{crit} = 140$ m/s to $U_{crit} = 120$ m/s. This change is similar to that which was observed for cold spray deposition of metals (Ref 31) and is consistent with trends in energy dissipation predicted for the impact of polymer particle on surfaces with mismatched moduli (Ref 15). Similar critical impact velocities, slightly below those of the melt-cast HDPE substrate, were also observed for both POM and PVC substrates. Here, a reduction in the critical impact velocity could be the result of the mismatch in moduli. However, the bonding mechanism between these very different polymers and the impacting HDPE particle is not entirely clear. It is important to note that all the data in Fig. 6 can still be well fit by the model in Eq 4, if the fitting parameter, k, is modified from $k = 0.55$, a value which has been shown to work for metals. The resulting values of the fitting parameter, k, are given in Table 1 and were found to range between $0.15 < k < 0.19$ with a mean value of $k = 0.166$ for all four of the polymeric substrates tested. As a result, on average, the critical impact velocity for deposition of HDPE is 3.3 times smaller than expected for a metal particle with the same material properties. Or expressed differently, a deposition of HDPE requires 11 times less kinetic energy than for a similar metal.

Perhaps the most notable difference between the like-on-like case and the different polymeric substrates that one can observe from the data in Fig. 6 is the appearance of an upper deposition boundary for the POM and PVC substrates. In the case of POM, erosion of the deposition was observed to occur through an interesting mechanism. During spraying at high impact velocities and pressures, a deposit appeared to form, build up, and then delaminate from the surface, repeating one or two times per second. At low temperatures, where this delamination effect was observed, deposition was not possible above $U_p > 150$ m/s

resulting in a very narrow deposition window. This observation suggests that for HDPE deposition on POM, once a threshold deposit size is attained, shear forces from the carrier gas can grow larger than the adhesion strength of the deposit. It also indicates that the adhesion strength between the HDPE and the POM is not optimal and suggests that the substrate material should be properly chosen to maximize adhesion strength of the subsequent deposition. Conversely, the failure of deposition of the HDPE particles on the PVC surface at high velocities occurred through a more commonly observed mechanism, which is the impact-induced ablation of the substrate. This observation suggests that, in this case, deposition was not possible due to a cohesive failure of the substrate material rather than an adhesive failure between the particles and the substrate.

Numerical Simulation of Particle Trajectory

Shock interactions, especially with the bow shock off the substrate, have been shown to negatively impact deposition efficiency (Ref 2, 32). We hypothesized that oblique shocks deflected the low-density polymer particles enough to negatively impact deposition efficiency. Numerical simulations, however, suggest that the complex gas dynamics of expansion/compression fans and oblique shocks have only a minor effect on the direction of particle impact. As a worst-case scenario, the shortest (7.21 mm) constant-area nozzle was drastically over-pressured with 72 psi, generating very strong expansion and compression fans and oblique shocks between the nozzle exit and substrate. At the nozzle exit, the gas accelerates nearly to Mach 3 and turns between +20° and −15° off-axis as it travels through the standoff region.

In order to capture the effects of radial variation in gas velocity, particles were released with an initial radial position, r_0 set in relation to the nozzle exit radius R. The ratio of initial position to nozzle radius r_0/R was chosen in the range $0.25 < r_0/R < 0.94$. The $r_0/R = 0.94$ case is an extreme case in which the particle is released a single particle diameter from the nozzle wall. To avoid modeling the focusing effect of flow through the converging portion of the nozzle, particles were instead released at the nozzle throat, with initial velocities set equal to the previously modeled centerline case. In Fig. 7, the resulting radial velocity of particles as they traverse the standoff region is shown. As the figure shows, the combination of inertia and brief residence time is such that the 48-μm particles pick up only a few meters/second of radial velocity (compared to axial velocity of 180-240 m/s). Even the most affected particle, released one particle diameter away from the nozzle wall, was deflected a mere 2.34° off an axis-parallel path over the course of the entire 12.7 mm standoff domain. The impingement angle at impact was 83.1° off the substrate plane or, equivalently, 6.9° off the centerline trajectory. Smaller particles were observed to be more greatly affected and achieved higher radial velocity components. A reduction in diameter by a factor of two resulted in about a factor of two increase in the radial velocity, but it was also accompanied by an increase in axial velocity (in this case, by about 17%). A 23-μm particle released at $r_0/R = 0.94$ impacts the substrate at a velocity angle of 11.7°, but if the release position was moved to $r_0/R = 0.6$, the angle at impact falls dramatically to 3.5°. While the literature shows that the presence of a bow shock reduces deposition efficiency, these simulations suggest that deflection from oblique shocks is not a likely cause of the lost deposition efficiency.

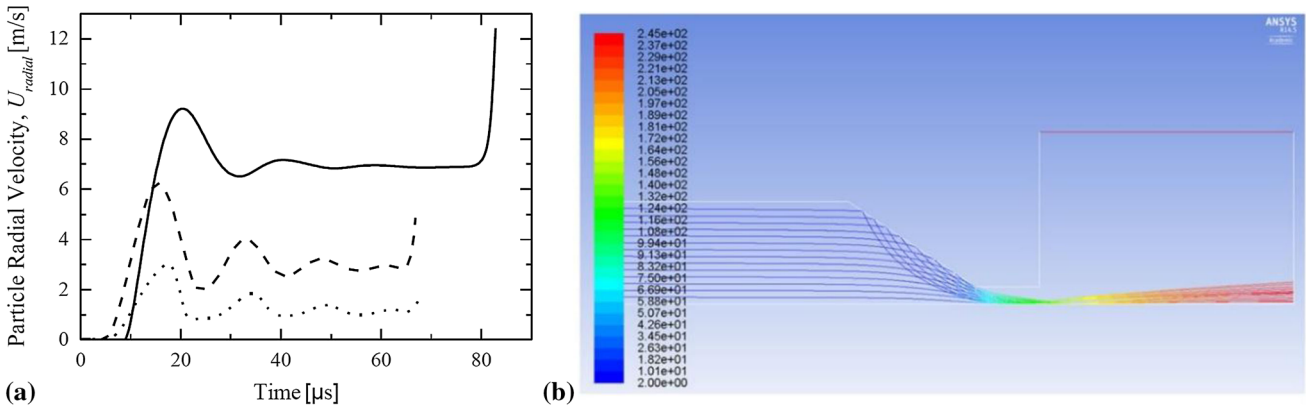

Fig. 7 Numerical simulation results showing the (a) radial velocity component of a 48-μm-diameter HDPE particles upon impact on the substrate for the flow shown in (b) exiting the Max Velocity Match Nozzle. In (a), the particles were released just upstream of the nozzle exit with initial velocities equal to the value along that streamline to avoid the particle focusing effects that can be observed in (b). The ratio r_0/R represents the fraction of nozzle exit radius R at which the particles were released. The data in (a) correspond to (–) $r_0/R = 0.94$, (– –) $r_0/R = 0.6$, and (···) $r_0/R = 0.25$. For reference, particle axial velocity was around 240 m/s for the two most central particles, and 180 m/s for the particle closest to the wall

Deposition Efficiency

In an earlier section, we showed that the critical velocity needed for the cold spray deposition of polymers is significantly lower than the critical velocity needed to deposit metal powders. This is true even if one factors in the differences in mechanical properties used to calculate the critical impact velocity using Eq 4. Unfortunately, another major difference between HDPE and metallic particles was a dramatic reduction in the deposition efficiency. For metallic particles, deposition efficiencies can approach 100%. For polymer particles, the only efficiencies reported to date were an unspecified value below 1% (Ref 2).

Differences in bonding mechanisms likely contribute to differences in deposition efficiency between polymers and metals. As discussed in the introduction, in cold spray of metals, the formation of metallurgical bonds across the interface is often credited as a potent source of adhesion strength (Ref 2, 20, 33). Polymeric materials, however, do not generally form such strong chemical bonds. Polyethylene, being nonpolar, is particularly inert, with its cohesive strength primarily provided by chain entanglement and overlap. In order to produce chain entanglement across the interface formed between the impacting particle and the substrate, it would seem that either mechanical mixing, melt fusion or significant diffusion must occur. The timescale of particle impacts, however, likely rules out a pure diffusive mechanism. Grujicic et al. (Ref 20) calculated that the typical metal–metal interdiffusion distance is between 0.004 and 0.1 nm at temperatures near the melting point and for the typical contact time during impact of 40 ns. Because this distance is only a fraction of the inter-atomic distance, they concluded that diffusion should not be considered a dominant mechanism. For HDPE and other polymers, the lower thermal diffusivity will lead to a larger temperature gradient upon impact, lower viscosities and enhanced diffusion after the particle impact. Together, this should lead to diffusion over a greater distance in polymers as compared to metals. However, the distance requirement is much larger for polymers than for metals. For metals, the inter-atomic distances are on the angstrom to nanometer scale in a metal lattice. However, for a polymer the more appropriate length scale is the radius of gyration of the polymer which can be tens of nanometers or more. Diffusive processes alone are, therefore, not likely the dominant contributor to the observed adhesion in cold spray of HDPE particles.

Some amount of mechanical mixing is therefore likely needed to induce interaction and entanglement between the polymer chains in particles and the polymer chains in the substrate. As shown by the simulation of Shah et al. (Ref 15), adhesion energy alone cannot explain polymer powder deposition in the cold spray process. At impact, the resulting shear rate can exceed $\dot{\gamma} = U_{\mathrm{pi}}/D_{\mathrm{p}} > 10^6\ \mathrm{s}^{-1}$. At these rates, the Weissenberg number, $Wi = \lambda\dot{\gamma}$, of the molten polymer within the zone of the adiabatic shear instability will be enormous, resulting in huge elastic stresses and perhaps even the onset of elastic flow instabilities, like elastic turbulence (Ref 34). These instabilities could drive mechanical mixing between the particle and substrate. Here, λ is the relaxation time of the molten polymer. Although the underlying mechanism of the particle deposition and bonding cannot be precisely determined from our experiments, we can begin to develop paths toward improvement in polymer cold spray deposition efficiency by investigating the role of a number of easily modified process parameters on deposition efficiency. These parameters include changes to particle temperature, impact velocity, and size; variation of the substrate material and temperature; and changes to the standoff distance between the nozzle and the substrate.

The deposition efficiency of 48-μm-diameter HDPE particles on an LDPE substrate is shown in Fig. 8 as a function particle impact velocities and standoff distance for hopper temperatures of $T_{\mathrm{H}} = 20$ °C (a) and $T_{\mathrm{H}} = 50$ °C (b). These two temperatures were chosen as

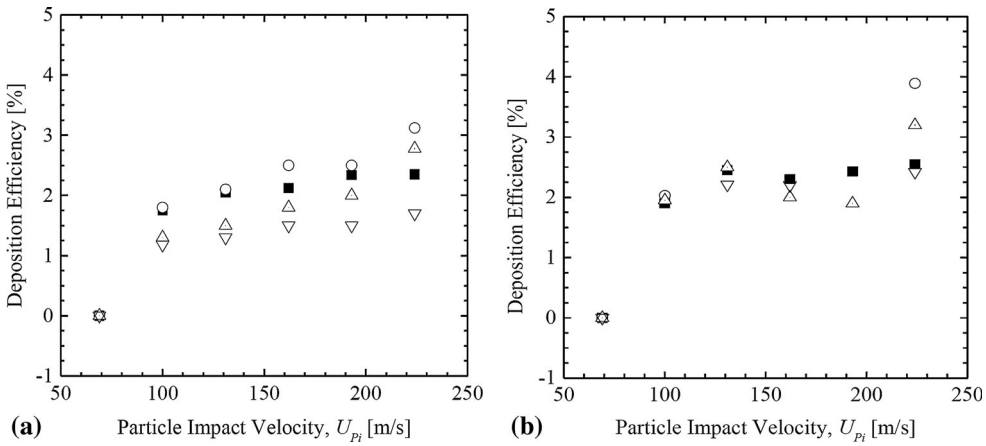

Fig. 8 Cold spray deposition efficiency of 48-μm-diameter HDPE particles on an LDPE substrate as a function of particle impact velocity at hopper temperatures of (a) $T_{\mathrm{H}} = 20$ °C and (b) $T_{\mathrm{H}} = 50$ °C. Data are included for standoff distances of $L_{\mathrm{SD}} = 5$ mm (■), $L_{\mathrm{SD}} = 10$ mm (○), $L_{\mathrm{SD}} = 15$ mm (▲), and $L_{\mathrm{SD}} = 20$ mm (▼)

representational to illustrate room temperature and roughly the maximum processing temperature of the hopper. For hopper temperature much beyond $T_H > 50$ °C, the HDPE particles became tacky and began to stick to each other within the hopper and to the walls of the hopper making smooth continuous processing difficult or impossible. No deposition was observed for particle impact velocities below a critical velocity of approximately $U_{pi} = 100$ m/s. Beyond this critical deposition velocity, particle deposition was observed with an initial deposition efficiency of between 1 and 2% depending on the processing conditions. The deposition efficiency was observed to increase monotonically with both increasing impact velocity and increasing hopper temperature. However, neither particle impact velocity nor hopper temperature had the desired dramatic effect on deposition efficiency. Take for example the case of the particle at $T_H = 20$ °C and a nozzle standoff distance of $L_{SD} = 10$ mm. For this case, increasing the particle impact velocity from $U_{pi} = 100$ m/s to $U_{pi} = 225$ m/s resulted in an increase in deposition efficiency from 1.8 to 3.2%. Similar increases, or near doubling, of the deposition efficiency were observed with the increase in particle impact velocities for all processing parameters studied. However, for these experiments, the maximum observed deposition efficiency was always found to be less than 4%. Increasing the hopper temperature from $T_H = 20$ °C to $T_H = 50$ °C had a modest effect, generally increasing deposition efficiency by only 0.2 to 0.5%. In both cases, the increase in deposition efficiency is likely the result of increased deformation of the particle and substrate during impact. For the case of increasing particle impact velocity, the more energetic impact likely resulted in an increase in heat dissipated during the plastic deformation of the particle and substrate during impact and a thermal softening or even localized melting of the impacting particle and substrate leading to adhesion (Ref 15). Increasing the hopper temperature had a similar effect as the particles begin and remain hotter throughout the nozzle and, upon impact, the polymer was more mobile, deformable, and closer to the melt temperature.

The effect of standoff distance was found to be non-monotonic. As seen in Fig. 8, an optimum standoff distance between the nozzle and the substrate was found to be approximately $L_{SD} = 10$ mm. With increasing standoff distance, the HDPE particles have more time to accelerate in the high-speed jet exiting the nozzle as seen in Fig. 1, but simultaneously, they have more time to cool to the temperature of the surrounding high-speed gas. These two effects are counterproductive as it is clear from Fig. 8 that increasing velocity and increasing, not decreasing, temperature improve deposition efficiency. The observed optimal standoff distance is not likely to be universal from one cold spray setup to the next, but will likely depend in some way on the complex flow profile downstream of the nozzle which for supersonic flows can include oblique shocks, expansion waves and bow shocks near the substrate.

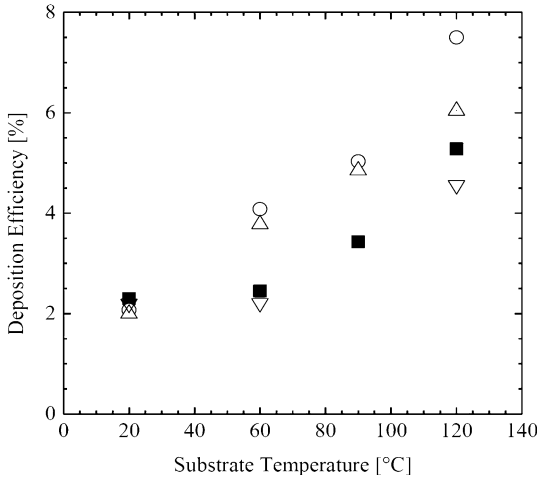

Fig. 9 Cold spray deposition efficiency of 48-μm-diameter HDPE particles on a LDPE substrate as a function of substrate temperature for a hopper temperature of $T_H = 50$ °C and a particle impact velocity of $U_{pi} = 162$ m/s. Data are included for standoff distances of $L_{SD} = 5$ mm (■), $L_{SD} = 10$ mm (○), $L_{SD} = 15$ mm (▲), and $L_{SD} = 20$ mm (▼)

The deposition efficiency data in Fig. 8(a) increase monotonically with increasing particle impact velocity. As a result, if we were to extrapolate the data to say 1000 m/s, which is near the limit of metal cold spray deposition, a deposition efficiency of less than 10% would still be expected. Thus, reaching a deposition efficiency of 100% by tuning only the particle temperature and the particle impact velocity does not appear to be feasible. Here, we use a linear fit to extrapolate the data with, which seems to fit the data well; however, there is evidence in the literature for metal powders that there is an exponential relationship between impact velocity and deposition efficiency (Ref 10). In Fig. 9, data are presented with a substrate heated from room temperature up to $T_s = 120$ °C. Note that the substrate temperatures quoted are measured from a thermocouple far from the deposition area and substrate temperature is controlled using a PCB (printed circuit board) heater on the moving stage. Because the high speed of the carrier gas downstream of the nozzle intensely cools down the substrate surface, the precise temperature below the impinging jet will be significantly colder than what is measured by the thermocouple and reported here. The objective of these experiments was to investigate the effect of enhancing the mobility the polymer chains within the substrate and, at the higher temperatures, using the heat from the substrate to enhance the mobility of the impacting HDPE particles. In Fig. 9, results showing the cold spray deposition efficiency of 48-μm-diameter HDPE particles

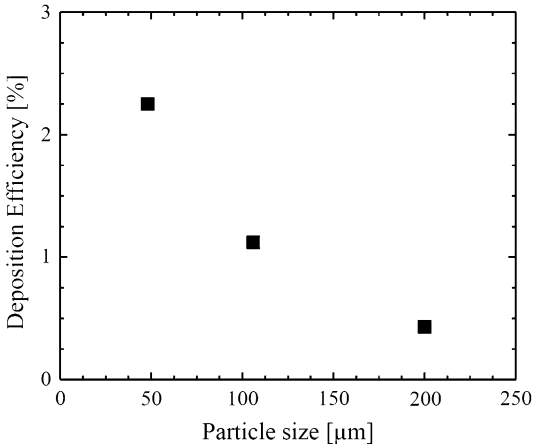

Fig. 10 Cold spray deposition efficiency on an LDPE substrate as a function of HDPE particle size for processing conditions involving a hopper temperature of $T_H = 50$ °C, a particle impact velocity of $U_{Pi} = 162$ m/s, a substrate temperature of $T_s = 20$ °C, and a standoff distance of $L_{SD} = 10$ mm

on an LDPE substrate are presented as a function of substrate temperature for a hopper temperature of $T_H = 50$ °C and a particle impact velocity of $U_{pi} = 162$ m/s. A comparison between figures 3.6 and 3.7 shows that heating the substrate influences deposition efficiency more significantly than heating the powder or increasing the impact velocity. At a standoff distance of $L_{SD} = 10$ mm, increasing the substrate temperature from $T_s = 20$ °C to $T_s = 120$ °C resulted in a nearly fourfold increase in the deposition efficiency from 2.1 to 7.6%.

It should also be noted that heating the substrate made it possible to deposit HDPE particles on inorganic substrates which was otherwise impossible. Under the processing conditions shown in Fig. 9 and a substrate temperature of $T_s = 120$ °C, successful deposition on glass with a deposition efficiency of 0.5% was achieved while deposition on aluminum with a deposition efficiency of 1.0% was possible. Ravi et al. (Ref 13) were also able to deposit high molecular weight polyethylene ceramic composites on aluminum only after they heated the aluminum substrate. This is thought to be because the creation of a molten layer of the polymer is a crucial step required before any low-temperature adhesion to aluminum take place (Ref 15).

Finally, we investigated the effect of particle size on deposition efficiency. In Fig. 10, cold spray deposition efficiency for HDPE particles with mean diameters of $D_p = 48$ μm, 106 μm and 200 μm on an LDPE substrate are plotted for a hopper temperature of $T_H = 50$ °C, a particle impact velocity of $U_{pi} = 162$ m/s, a substrate temperature of $T_s = 20$ °C and a standoff distance of $L_{SD} = 10$ mm. Decreasing the particle size significantly improves deposition efficiency. By decreasing particle size from 200 to 48 μm, the deposition efficiency was found to increase from 0.45 to 2.3%. This increase is roughly inversely proportional to the particles size, $DE \propto 1/D_p$. This observation is consistent with predictions of numerical simulations and can be understood through the development of a simple theory.

In previous numerical studies, mechanics of metal and polymeric particle impacts have been shown to strongly depend on the ratio of the kinetic energy per unit volume of the particle at the time of impact to the plastic strain energy density (Ref 6, 15, 35). This non-dimensional parameter is expressed as $\rho U_{pi}/\sigma_Y$ where σ_Y is the substrate's dynamic yield strength. Thus, the deformation of the particles upon impact is expected to be independent of the particle diameter if the material behavior is rate independent and the gravitational effects are negligible. The gravitational effects can be considered negligible because we are dealing with micron-sized bodies. The material properties of the particle and substrate are rate dependent; however, numerical simulations of HDPE particle impacts showed little difference in particle deformation even as the particle size was increased by an order of magnitude from 50 to 500 μm (Ref 15). The net result was more than 90% of the kinetic energy of the impacting particle dissipated as heat due to the plastic deformation of the particle and the substrate. Unfortunately, even though the same fraction of kinetic energy was dissipated for all particle sizes, the kinetic energy upon impact, and thus the non-dissipated kinetic energy remaining in the particle after impact, will grow like the mass or volume of the particle, $KE_{ND} \propto D_p^3$. For the particle to deposit on the substrate, the work of adhesion between the particle and substrate must be larger than the remaining kinetic energy in the particle, $W_{PS} > -KE_{ND}$. The work of adhesion will grow with the cross-sectional area of the impact crater formed between the impacting particle and the substrate which is proportional to the square of the particle diameter, $W_{PS} \propto D_p^2$. Thus, for the same processing conditions, decreasing particle size is expected to make deposition more likely as the relative importance of work of adhesion to non-dissipated impact kinetic energy grows inversely proportional to particle size, $W_{PS}/KE_{ND} \propto 1/D_p$, just as deposition efficiency was observed to do. These observations would suggest that a possible path toward more efficient deposition would involve the use of even smaller particles. However, it is expected that at some small diameter the reduction in particle mass and inertial will allow them to be deflected away from the surface by the bow shocks and pressure gradients near the substrate where the impinging jet stagnates. Future studies are planned to test the lower limit of particle size.

Conclusions

In this work, a combined computational and experimental study was employed to study the cold spray deposition of high-density polyethylene powders over a wide range of particle temperatures and impact velocities. Cold spray deposition of polyethylene powders was successfully demonstrated across a range broad range of substrate materials including several different polymer substrates with different moduli. Cold spray deposition of polyethylene powders was also demonstrated on inorganic substrates like glass and aluminum. The resulting deposits had little to no porosity. A material-dependent window of successful deposition was determined for each substrate as a function of particle temperature and impact velocity. These deposition maps allowed deeper comparison of polymer deposition with reported metal cold spray results, uncovering aspects of similarity as well as substantial difference.

Like the cold spray deposition of metallic particles, the critical impact velocity, above which successful deposition was observed, was shown to decrease with increasing temperature of the HDPE particles. Additionally, like metals, a mismatch between the modulus of the particle and the substrate was found to be beneficial for particle deposition, resulting in a decrease in the critical impact velocity. Unlike the cold spray deposition of metallic particles, the empirical model used to predict the critical impact velocity for metallic particles was found to vastly overpredict the particle velocities and kinetic energy necessary to achieve deposition. For the HDPE particles used in these studies, the critical impact velocity was found to be in the range of $U_{pi} = 100\text{-}50$ m/s, while the predictions of the empirical model used in metal cold spray predicted a value that was a factor of three larger between 300 and 450 m/s.

Despite the reduced particle velocity and kinetic energy demands, the maximum deposition efficiency reported by literature on polymer cold spray was less than 1% (Ref 2). This deposition efficiency is much smaller than what has been reported for metallic cold spray. In the present study, a detailed investigation into the deposition efficiency over a wide range of processing conditions was performed. The processing conditions varied included the particle temperature, particle impact velocity, particle size, substrate material, substrate temperature, and the standoff distance between the nozzle and the substrate. The present study revealed that increasing particle temperature, particle impact velocity, and substrate temperature, all had a positive effect on deposition efficiency. Additionally, reducing particle size was also shown to have a dramatic effect on deposition efficiency. The standoff distance between the nozzle and the substrate had a non-monotonic effect. An optimal distance was observed that balances the acceleration of the particle with its cooling during its time of flight. By optimizing operational parameters, deposition efficiency of close to 10% was achieved for the cold spray deposition of HDPE particles. This represents an order of magnitude improvement on the best results presented in the literature.

Acknowledgments This research was accomplished through a cooperative research agreement with the US Army Research Laboratory, Contract: W911NF-15-2-0024, 'Intelligent Processing of Materials by Design.'

References

1. A. Papyrin, V. Kosarev, S. Klinkov, A. Alkhimov, and V.M. Fomin, *Cold Spray Technology*, Elsevier, Amsterdam, 2007
2. Y. Xu and I.M. Hutchings, Cold Spray Deposition of Thermoplastic Powder, *Surf. Coat. Technol.*, 2006, **201**(6), p 3044-3050
3. T. Schmidt, F. Gartner, H. Assadi, and H. Kreye, Development of a Generalized Parameter Window for Cold Spray Deposition, *Acta Mater.*, 2006, **54**, p 729-742
4. W.O.R. Lupoi, Deposition of Metallic Coatings on Polymer Surfaces Using Cold Spray, *Surf. Coat. Technol.*, 2010, **205**, p 2167-2173
5. C.R.C. Lima, N.F.C. de Souza, and F. Camargo, Study of Wear and Corrosion Performance of Thermal Sprayed Engineering Polymers, *Surf. Coat. Technol.*, 2013, **220**, p 140-143
6. S.M. Baran Yildirim and A. Gouldstone, Modeling of High Velocity Impact of Spherical Particles, *Wear*, 2011, **270**(2011), p 703-713
7. J.A. Zukas, *High-Velocity Impact Dynamics*, Wiley, New York, 1990
8. V.K. Champagne, *The Cold Spray Materials Depostion Process: Fundamentals and Applications*, Woodhead Publishing, Cambridge, 2007
9. M. Gardon, A. Latorre, M. Torrell, S. Dosta, J. Fernández, and J.M. Guilemany, Cold Gas Spray Titanium Coatings onto a Biocompatible Polymer, *Mater. Lett.*, 2013, **106**, p 97-99
10. H. Assadi, T. Schmidt, H. Richter, J.-O. Kliemann, K. Binder, F. Gartner, T. Klassen, and H. Kreye, On Parameter Selection in Cold Spraying, *Therm. Spray Technol.*, 2011, **20**, p 1161-1176
11. V.K. Champagne, The Repair of Magnesium Rotorcraft Components by Cold Spray, *J. Fail. Anal. Prev.*, 2008, **8**, p 164-175
12. A.M. Vilardell, N. Cinca, and A. Concustell, Cold Spray as an Emerging Technology for Biocompatible and Antibacterial Coatings: State of Art, *Mater. Sci.*, 2015, **50**, p 4441
13. K. Ravi, Y. Ichikawa, T. Deplancke, K. Ogawa, O. Lame, and J.-Y. Cavaille, Development of Ultra-High Molecular Weight Polyethylene (UHMWPE) Coating by Cold Spray Technique, *J. Therm. Spray Technol.*, 2015, **24**(6), p 1015-1025
14. A.S. Alhulaifi, G.A. Buck, and W.J. Arbegast, Numerical and Experimental Investigation of Cold Spray Gas Dynamic Effects for Polymer Coating, *J. Therm. Spray Technol.*, 2012, **21**, p 852-862
15. S. Shah, J. Lee, and J.P. Rothstein, Numerical Simulations of the High Velocity Impact of a Single Polymer Particle During Cold Spray Deposition, *J. Therm. Spray Technol.* (2016)
16. T. Hussain, Cold Spraying of Titanium: A Review of Bonding Mechanisms, Microstructure and Properties, *Key Eng. Mater.*, 2013, **533**, p 53-90

17. H. Assadi, F. Gärtner, T. Stoltenhoff, and H. Kreye, Bonding Mechanism in Cold Gas Spraying, *Acta Mater.*, 2003, **51**, p 4379-4394
18. W.-Y. Li, C. Zhang, X. Guo, C.-J. Li, H. Liao, and C. Coddet, Study on Impact Fusion at Particle Interfaces and its Effect on Coating Microstructure in Cold Spraying, *Appl. Surf. Sci.*, 2007, **254**, p 517
19. W.-Y. Li, C. Zhang, H.-T. Wang, X.P. Guo, and H.L. Liao, C.-J. Li., Significant Influences of Metal Reactivity and Oxide Films at Particle Surfaces on Coating Microstructure in Cold Spraying, *Appl. Surf. Sci.*, 2007, **253**, p 3557
20. S.V. Klinkov, V.F. Kosarev, and M. Rein, Cold Spray Deposition: Significance of Particle Impact Phenomena, *Aerosp. Sci. Technol.*, 2005, **9**, p 582-591
21. T. Hussain, D.G. McCartney, P.H. Shipway, and D. Zhang, Bonding Mechanisms in Cold Spraying: The Contributions of Metallurgical and Mechanical Components, *Therm. Spray Technol.*, 2009, **18**, p 364-379
22. M. Grujicic, J.R. Saylor, D.E. Beasley, W.S. Derosset, and D. Helfritch, Computational Analysis of the Interfacial Bonding between Feed-Powder Particles and the Substrate in the Cold-Gas Dynamic-Spray Process, *Appl. Surf. Sci.*, 2003, **219**, p 211-227
23. C.-S. Yih, Instability Due to Viscosity Stratification, *J. Fluid Mech.*, 1967, **27**, p 337-352
24. A. Concustell, J. Henao, S. Dosta, N. Cinca, I.G. Cano, and J.M. Guilemany, On the Formation of Metallic Glass Coatings by Means of Cold Gas Spray Technology, *J. Alloys Comp.*, 2015, **651**, p 764-772
25. J. Henao, A. Concustell, S. Dosta, G. Bolelli, I.G. Cano, L. Lusvarghi, and J.M. Guilemany, Deposition Mechanisms of Metallic Glass Particles by Cold Gas Spraying, *Acta Mater.*, 2017, **125**, p 327-339
26. V.K. Champagne, D.J. Helfritch, S.P.G. Dinavahi, and P.F. Leyman, Theoretical and Experimental Particle Velocity in Cold Spray, *Therm. Spray Technol.*, 2011, **20**, p 425-431
27. A.H. Shapiro, *The Dynamics and Thermodynamics of Compressible Fluid Flow*, The Ronald Press Company, New York, 1953
28. J.H. Lienhard, *A Heat Transfer Textbook*, Prentice-Hall, Upper Saddle River, 1981
29. G.M. Swallowe, *Mechanical Properties and Testing of Polymers an A-Z Reference*, Springer Netherlands, Dordrecht, 1999
30. G.M. Swallowe, *Adiabatic Shear Instability: Theory. Mechanical Properties and Testing of Polymers an A-Z Reference*, Springer, Dordrecht, 1999
31. G. Bae, Y. Xiong, S. Kumar, K. Kang, and C. Lee, General Aspects of Interface Bonding in Kinetic Sprayed Coatings, *Acta Mater.*, 2008, **17**, p 4858-4868
32. J. Pattison, S. Celotto, A. Khan, and W. O'Neill, Standoff Distance and Bow Shock Phenomena in the Cold Spray Process, *Surf. Coat. Technol.*, 2008, **202**, p 1443-1454
33. M. Grujicic, C.L. Zhao, W.S. DeRosset, and D. Helfritch, Adiabatic Shear Instability Based Mechanism for Particles/Substrate Bonding in the Cold-Gas Dynamic-Spray Process, *Mater. Des.*, 2004, **25**, p 681-688
34. A. Groisman and V. Steinberg, Elastic Turbulence in a Polymer Solution Flow, *Nature*, 2000, **405**, p 53-55
35. K.L. Johnson, *Contact Mechanics*, Cambridge University Press, Cambridge, 1985